Journal of Computational Physics 227 (2008) 8145–8164

Contents lists available at ScienceDirect

Journal of Computational Physics

journal homepage: www.elsevier.com/locate/jcp

Effective numerical viscosity in spectral multidomain penalty method-based simulations of localized turbulence

P.J. Diamessis [a,*], Y.C. Lin [b], J.A. Domaradzki [b]

[a] School of Civil and Environmental Engineering, Cornell University, 220 Hollister Hall, Ithaca, NY 14853, United States
[b] Department of Aerospace and Mechanical Engineering, University of Southern California, Los Angeles, CA 90089-1191, United States

ARTICLE INFO

Article history:
Received 18 October 2007
Received in revised form 25 April 2008
Accepted 20 May 2008
Available online 7 July 2008

Keywords:
Spectral multidomain
Penalty methods
Spectral filtering
Under-resolution
Numerical viscosity
Turbulence

ABSTRACT

The numerical dissipation operating in a specific spectral multidomain method model developed for the simulation of incompressible high Reynolds number turbulence in doubly periodic domains is investigated. The method employs Fourier discretization in the horizontal directions and the discretization in the vertical direction is based on a Legendre collocation scheme local to each subdomain. Both spatial discretizations are characterized by either no or near-negligible artificial dissipation. In high Reynolds number simulations, which are inherently under-resolved, stability of the numerical scheme is ensured through spectral filtering in all three directions and the implementation of a penalty scheme in the vertical direction. The dissipative effects of these stabilizers are quantified in terms of the numerical viscosity, using a generalization of the method previously employed to analyze numerical codes for the simulation of homogeneous, isotropic turbulence in triply periodic domains. Data from simulations of the turbulent wake of a towed sphere are examined at two different Reynolds numbers varying by a factor of twenty. The effects of the stabilizers are found to be significant, i.e. comparable, and sometimes larger, than the effects of the physical (molecular) viscosity. Away from subdomain interfaces, the stabilizers have an expected dissipative character extending over a range of scales determined by timestep and the degree of under-resolution, i.e. Reynolds number. At the interfaces, the stabilizers tend to exhibit a strong anti-dissipative character. Such behavior is attributed to the inherently discontinuous formulation of the penalty scheme, which suppresses catastrophic Gibbs oscillations by enforcing C_0 and C_1 continuity only weakly at the interfaces.

1. Introduction

Incompressible turbulent flows are governed by the Navier–Stokes equations

$$\frac{\partial \mathbf{u}}{\partial t} + \mathbf{u} \cdot \nabla \mathbf{u} = -\frac{1}{\rho_0} \nabla p + \nu \nabla^2 \mathbf{u} + \mathbf{F}, \tag{1}$$

$$\nabla \cdot \mathbf{u} = 0, \tag{2}$$

where $\mathbf{u}(\mathbf{x}, t)$ is the velocity field, $u_i = (u_1, u_2, u_3) = (u, v, w)$, ν is the kinematic viscosity, p is the pressure, ρ_0 is the density (assumed constant in this study) and $\mathbf{F}$ is a forcing.

* Corresponding author. Tel.: +1 607 255 1719; fax: +1 60 255 9004.
E-mail addresses: pjd38@cornell.edu (P.J. Diamessis), yunchenl@usc.edu (Y.C. Lin), jad@usc.edu (J.A. Domaradzki).

0021-9991/$ - see front matter © 2008 Elsevier Inc. All rights reserved.
doi:10.1016/j.jcp.2008.05.011

In solving numerically Eqs. (1) and (2) for increasing Reynolds numbers[1] one quickly encounters a difficulty that resolving all physically relevant scales of motion is not possible because of a demanding scaling of computational work as Reynolds number grows [38]. If an attempt is made to numerically solve the governing equations with a resolution inadequate to capture all active modes of freedom the numerics become unstable or, if no instability is encountered, the obtained solution may be physically inaccurate. In practice, these difficulties are addressed in two distinct ways. One is based on modeling of the effects of unresolved modes on the resolved ones using knowledge of the physics of turbulence. This leads to modified equations containing explicit turbulence modeling terms as in Reynolds Averaged Navier–Stokes (RANS) and Large Eddy Simulations (LES) techniques. Reviews of such physically motivated turbulence modeling methods are provided in [38,32,37,34,12]. Another focuses on monitoring and controlling instabilities using procedures of numerical nature such as filtering, employing explicit or implicit artificial dissipation and adding hyperviscosity terms [4,5,19,6]. Both approaches often can be characterized as an introduction of an additional dissipation into the equations. This is usually obvious for the turbulence modeling approaches because they are most frequently based on the eddy viscosity concept. For the numerical stabilization methods, particularly implicit as in the Monotonically Integrated LES (MILES) [3,21], it is less apparent. In MILES one discretizes directly Navier–Stokes equations (1) and (2) using higher-order non-oscillatory methods, often referred to as monotonicity or shape preserving, shock capturing, or briefly, monotone schemes; e.g. total variation diminishing, TVD, flux-corrected-transport, FCT, and various flux-limited and sign-preserving schemes [44,49,23]. The MILES method is based on the observation that truncation errors in such discretizations of Navier–Stokes equations introduce numerical dissipation with the implicit effects of the discretization qualitatively similar to the effects of the explicit turbulence models. This similarity, observed in a number of individual simulations, led to the emergence of a class of methods currently known simply as Implicit LES (ILES). A modern review of the subject can be found in a monograph edited by Grinstein et al. [20].

The success of a particular ILES method depends critically on how well the numerical dissipation approximates the actual SGS dissipation due to turbulence physics. Yet despite its importance only recently has a method been proposed to quantify the numerical dissipation of stabilization procedures in terms of the numerical eddy viscosity [13]. The method has been used [13,14] to quantify the properties of the implicit dissipation acting in a specific non-oscillatory finite volume solver MPDATA [41]. It has also been employed in a task of designing a numerical scheme with prescribed dissipative properties [27]. In both cases analysis was performed for isotropic turbulence simulations in domains with triply periodic boundary conditions. This paper is motivated by the recognition that the numerical dissipation is ubiquitous in numerical simulations of high Reynolds number flows and, consequently, by the need to develop more general tools that would allow to analyze it for flows other than isotropic turbulence. We will focus here on a nominally high-order spectral multidomain/element scheme that was developed for a specific problem of simulating stratified wakes.

When high-order accuracy spectral/spectral element discretization schemes based on orthogonal polynomials are employed, the artificial dissipation associated with the truncation error is either non-existent (Fourier trigonometric polynomials) or diminishes exponentially with increasing order of polynomial approximation (Legendre and Chebyshev polynomials) [5]. In a Direct Numerical Simulation (DNS), which is intrinsically well-resolved, use of such high-order weakly/non-dissipative schemes enables the highly accurate evaluation of dissipation and mixing at the smallest scales of the flow, where molecular viscosity is the only damping mechanism. Nevertheless, to extend the range of governing parameters where such methods can be applied to produce numerically stable and physically realistic results in the framework of under-resolved fluid flow simulations, various numerical procedures are used. Numerical stability is ensured through explicit spectral filtering (or its surrogate, a hyperviscous operator of the same order introduced in the governing equation) [33,29] which is sufficient when a Fourier discretization is used. If an element-based discretization is employed in one or more directions, typically using Legendre polynomials, the stability enabled by spectral filtering is further buttressed through a discontinuous formulation, i.e. discontinuous Galerkin [17] or a penalty multidomain collocation scheme [24,8].

In this higher-order variant of the MILES approach, the numerical viscosity associated with spectral filtering is described as a function of $N^{-(p-1)}$ [19,16], where N is the order of polynomial approximation and p is the filter order, with no physical units attached to it [19,16]. In work using a hyperviscous operator, the numerical viscosity has been alternatively defined as UL^{p-1}/Re_p [47], where U and L are characteristic velocity and lengthscales of the flow, respectively, and Re_p is an externally imposed quantity set to 10^{-33}, i.e. below machine precision. In simulations of shock-turbulence interactions Cook and Cabot [6] introduce grid dependent numerical viscosities with coefficients optimized empirically to fit a number of test problems.

Since the above stabilization techniques have generally a dissipative character, it is natural to inquire whether their effects offset the advantages afforded by weakly dissipative/non-dissipative spatial discretizations. Specifically, it is of interest to examine how these effects compare with the effects of an actual molecular dissipation. This question can be conveniently reformulated as a comparison between the numerical and the molecular viscosity, because the latter is constant in a given simulation. However, the stabilization techniques rarely have the same form as the molecular viscous term so a direct comparison of an artificial and a molecular viscosity is not possible. Also, as noted above, the numerical viscosity optimized for a given scheme may not have an unambiguous measure of its units to allow comparison with its molecular counterpart. Moreover, a dependence of the numerical viscosity on spatial scale can not be easily inferred. This paper attempts to address these shortcomings by extending the numerical eddy viscosity analysis applied to MPDATA [13,14] (in triply periodic domains) to

[1] The Reynolds number may be defined here in terms of some characteristic geometric lengthscale and large-scale velocity.

a spectral multidomain method (in a domain with one non-periodic direction) that uses penalty techniques and spectral filtering to achieve stable results in numerical simulations of high Reynolds number incompressible flows.

It should be emphasized that, although desirable, a rigorous mathematical analysis leading to detailed parameterizations of numerical viscosity in under-resolved spectral multidomain penalty method-based simulations as a function of Reynolds number, order of polynomial approximation N, subdomain size h and filter order p cannot be easily accomplished. Although such an analysis may be feasible in the context of a linear advection/diffusion equation or a single non-linear equation (e.g. Burgers or Korteweg-DeVries) with analytically prescribed initial conditions, its application to the incompressible Navier–Stokes equations is made significantly more complex by equation coupling, boundary conditions and geometry, large-scale forcing and turbulent initial conditions. This paper has the more modest objective of outlining a procedure for estimating the numerical viscosity, and in the process allowing a direct comparison with the molecular viscosity, for high-order schemes (designed for domains with one non-periodic direction) using numerical stabilization techniques. The example considered in this paper provides a quantitative appreciation of the dissipative contributions of spectral filtering and penalty methods to a specific set of simulations of turbulent wakes [11]. Such an appreciation is expected to allow a more robust assessment of the capability of the stabilized spectral multidomain scheme under consideration to simulate fluid flow phenomena that cannot be simulated by lower order methods, e.g., the physics of localized regions with nearly inviscid dynamics at high Reynolds numbers. This capability has already been demonstrated by the observation of secondary instabilities in stratified turbulent wakes [10] and instabilities of internal solitary wave-induced boundary layers [9], phenomena which corresponding simulations based on low-order finite difference schemes [15,43] have been unable to capture. Finally, the analysis method can be easily extended to other codes if a baseline "non-dissipative" simulation (defined and described in Section 5) can be constructed.

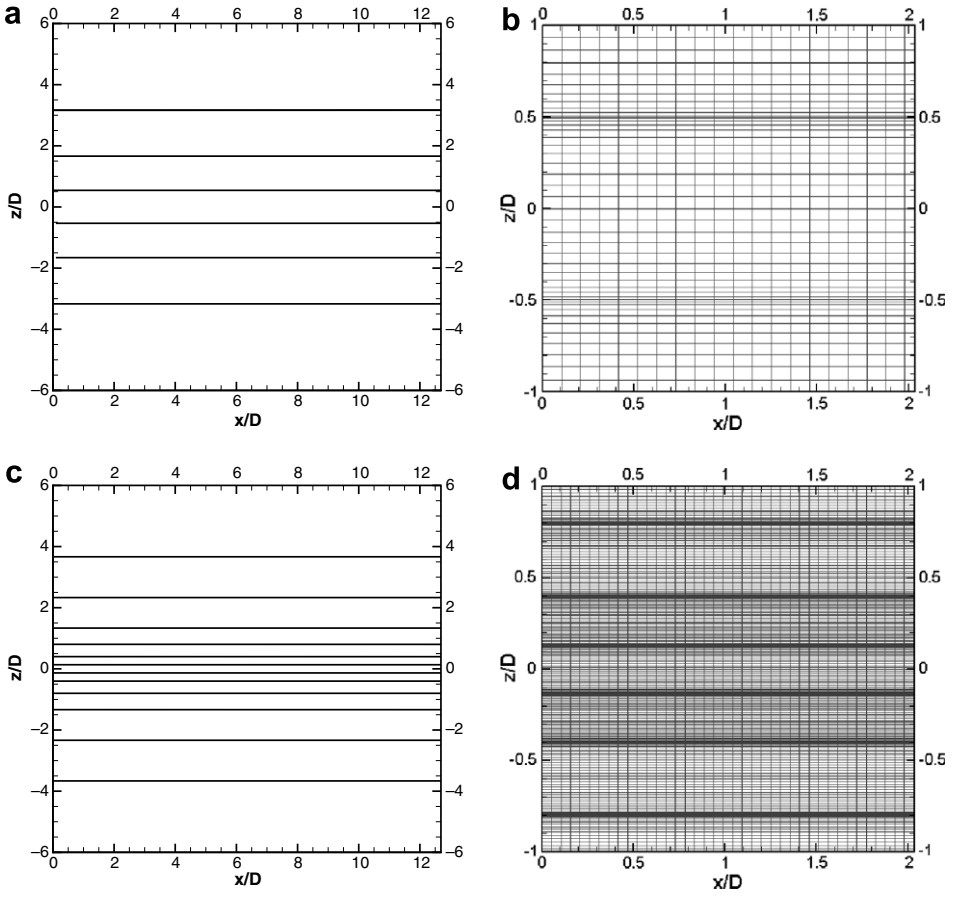

Fig. 1. Streamwise truncated Oxz section of the numerical grid employed in this study for the DNS of a stratified turbulent wake. The top and bottom row show grid used for the simulations at $Re = 5 \times 10^3$ and $Re = 10^5$, respectively. The left column shows the full extent of the computational domain for each Re. The black solid lines delineate subdomain interfaces with the local GLL grid omitted for clarity. The right column shows an exploded view of the wake core region for each Re with the local GLL grid included. The $Re = 5 \times 10^3$ run employs $M = 7$ subdomains of order of approximation $N = 24$, with subdomain origins located at $z/D = -6, -3.17, -1.67, -0.5, 0.5, 1.67$ and 3.17. The $Re = 10^5$ run employs $M = 13$ subdomains of order of approximation $N = 40$, with subdomain origins located at $z/D = -6, -3.67, -2.33, -1.33, -0.8, -0.4, -0.13, 0.13, 0.4, 0.8, 1.33, 2.33$ and 3.67.

Following a brief overview of the numerical method, stabilizers employed therein and the specific simulations considered, the numerical eddy viscosity analysis is elaborated upon in Section 5. Results are then presented in Section 6. Conclusions and possible extensions of this work, including directions for a more rigorous analysis, are given in Section 7.

2. Numerical method

In this study, the three-dimensional incompressible Navier–Stokes equations (1) and (2) are recast in skew-symmetric form [7]:

$$\frac{\partial \mathbf{u}}{\partial t} = \underbrace{-\frac{1}{2}[\mathbf{u}\cdot\nabla\mathbf{u} + \nabla(\mathbf{u}\cdot\mathbf{u})]}_{\mathbf{N}(\mathbf{u})} - \frac{1}{\rho_0}\nabla p + \nu \underbrace{\nabla^2\mathbf{u}}_{\mathbf{L}(\mathbf{u})}, \tag{3}$$

$$\nabla\cdot\mathbf{u} = 0. \tag{4}$$

Periodic boundary conditions are used in both horizontal directions. In the vertical direction, non-slip and free-slip boundary conditions are employed at the bottom and top of the computational domain, respectively.

The temporal discretization of (3) and (4) consists of three fractional steps [8]: the explicit treatment of the non-linear terms, the implicit solution of a Poisson equation for the pseudo-pressure, which ensures an incompressible velocity field, and the implicit solution of a Helmholtz equation for the viscous terms, where the physical boundary conditions are imposed. This splitting approach combines third-order stiffly stable and backward-differentiation schemes with a dynamic high-order boundary condition for the pressure. Thus, $O(\Delta t^2)$ accuracy is ensured for both velocity and pressure [22] and the maximum possible value of stable timestep is attainable [30].

In the periodic horizontal directions, Fourier spectral discretization is used with N_x and N_y Fourier modes in the longitudinal and spanwise direction, respectively. In the vertical direction, the computational domain is partitioned into M subdomains of variable height H_k $(k = 1,\ldots M)$ and fixed order of polynomial approximation N (Fig. 1). The total number of vertical grid points is $N_z = M(N+1)+1$. Within each subdomain, a spectral collocation scheme based on Legendre polynomials [7] is used. Subdomains communicate with their neighbors via a simple patching condition [8]. The multidomain scheme allows for increased vertical resolution in the turbulent core of the wake while also resolving adequately, yet not excessively, the internal wave-dominated ambient.

The resolutions used in this paper aim to capture the dynamically relevant scales of motion in the wake while accomodating available computational resources and the need for rapid run turnaround. As a result, the DNS become under-resolved at higher Reynolds numbers and the effect of molecular viscosity is felt only weakly by the resolved scales. When spectral schemes, which are inherently non-dissipative, are used in under-resolved simulations, the resulting Gibbs oscillations are compounded by aliasing effects driven by the non-linear term, leading to catastrophic numerical instabilities [19]. In the present model, two techniques are used to ensure stability of the numerical solution while preserving spectral accuracy: explicit spectral filtering and penalty schemes.

3. Stabilization techniques

3.1. Penalty methods

Penalty methods consist of collocating a linear combination of the equation and boundary/patching conditions (the latter multiplied by a penalty coefficient) at the boundaries/subdomain interfaces, respectively [25,24]. At the subdomain interfaces, patching conditions are treated as boundary conditions local to the specific subdomain [24]. The equation is satisfied arbitrarily close to the boundary/subdomain interface, with near negligible error at these locations, thereby enabling the stable computation of the high *Re* "internal" (internal with respect to the subdomain boundary) dynamics of the flow without having to resolve the thin numerical/viscous physical boundary layers or sharp gradients at subdomain interfaces [8]. The weak enforcement of boundary/patching conditions renders the penalty method inherently discontinuous, i.e. any physical location on a subdomain interface has a separate grid point assigned to it on each contributing subdomain. The difference in solution values at each of these grid points is of the order of the discretization scheme [24].

In terms of the splitting scheme summarized in Section 2, the penalty method is applied at two different levels in the incompressible Navier–Stokes equations. The explicit non-linear term advancement is treated as a hyperbolic equation whereas the implicit viscous term treatment as a parabolic equation (in this section all subsequent equations are written as a function of the u-velocity without loss of generality):

$$\frac{\partial u}{\partial t} = \mathbf{N}(u), \tag{5}$$

$$\frac{\partial u}{\partial t} = \nu\mathbf{L}(u). \tag{6}$$

The temporal derivatives in Eqs. (5) and (6) are only approximations to their discrete counterparts appearing in the respective fractional steps of the temporal discretization under consideration.

The penalty formulation of Eq. (5), in physical space, for each subdomain of index-k and uniform order N is

$$\frac{\partial u^k}{\partial t} = \mathbf{N}(u^k) - \tau_1^k Q_k^-(z_i^k)[\alpha u_0^k - g_1^k(t)] - \tau_2^k Q_k^+(z_i^k)[\gamma u_N^k - g_2^k(t)], \tag{7}$$

where

$$Q_k^-(z_i^k) = \delta_{i0}, \quad Q_k^+(z_i^k) = \delta_{iN} \tag{8}$$

here δ_{ij} is the Kronecker delta function with subscript i corresponding to the collocation point z_i^k. The values of the coefficients α, γ, τ_1^k and τ_2^k are determined by treating each individual subdomain as a single domain whose interfaces support patching conditions that act as open boundary conditions through which information is exchanged with adjacent subdomains. The patching conditions are the terms in the brackets of Eq. (7) and are treated as localized open boundary conditions where each subdomain experiences "inflow" or "outflow" depending on the value of the vertical interfacial velocities W_0^k and W_N^k at the previous timesteps, thereby setting the specific form of $g_1^k(t)$ and $g_2^k(t)$ (see also Refs. [25,24,8]). Note that, due to the use of no-slip and free-slip boundary conditions at the bottom and top, respectively, of the computational domain, the penalty operators in Eq. (5) are set to zero at the top and bottom boundaries.

The penalty formulation of (6) is significantly different from that of (5) due to its parabolic nature. In Fourier space, for an individual horizontal wavenumber pair (k_x, k_y), the final equation is

$$\epsilon \frac{\mathrm{d}^2}{\mathrm{d}z^2} u - u + F - \tau_1^k Q_k^-(z_i^k)\left[\alpha u_0^k - \beta\epsilon \frac{\partial u_0^k}{\partial z^k} - g_1^k(t)\right] - \tau_2^k Q_k^+(z_i^k)\left[\gamma u_{N_k}^k + \delta\epsilon \frac{\partial u_N^k}{\partial z^k} - g_2^k(t)\right] = 0. \tag{9}$$

The first three terms in the left-hand side of (9) originate from the discretization of (6) in Fourier space with F carrying information from the previous fractional step, i.e. the treatment of the pressure. The small parameter ϵ is defined in [8] and scales as $\nu\Delta t$. $Q_k^-(z_i^k)$ and $Q_k^+(z_i^k)$ are defined in (8). Again, the terms in the brackets represent appropriate patching or boundary operators, defined in detail in Diamessis et al. [8]. The coefficients α, β, γ and δ are chosen to represent either the externally imposed boundary condition (Dirichlet, Neumann or Robin) or are set to unity at the subdomain interfaces where the patching condition corresponds to a localized Robin boundary condition. The penalty coefficient values are then set accordingly.

3.2. Spectral filters

Penalty schemes are designed to ensure numerical stability in the vicinity of subdomain interfaces and tend to be less effective in the subdomain interiors. The initial objective of the turbulent wake simulations described in this paper was to reproduce wakes observed in the laboratory at $Re \approx 5 \times 10^3$ (where Re is defined in Section 4.3 to be based on body diameter and tow speed) [42] while balancing adequate resolution of the energy-containing scales of the flow and a run turnaround of wall-clock time of no more than a day. To this end, a resolution of $128 \times 64 \times 119$ on an MPI-parallelized code was deemed sufficient (see also the relevant discussion in Section 4.3). At this resolution, numerical tests performed by the authors using the spectral multidomain penalty scheme as the only stabilization technique, indicated that the increased stability enabled by the scheme allowed an increase of the maximum attainable Re from 50 to 500. When the value of Re, and thus, the degree of under-resolution, was increased beyond approximately 10^3, high-wavenumber numerical noise of increasing amplitude, enhanced by the non-linearity of the Navier–Stokes equations through aliasing, emerged in the subdomain interiors and destabilized the simulations. To suppress this numerical noise, a low-pass spectral filter is applied to the modal expansion of the numerical solution, whose spectral accuracy is thereby minimally impacted [33]. At the higher $Re = 10^5$ runs considered in this work, a judicious choice of resolution and filter strength is made to exploit the distinct advantages of high accuracy and minimal artificial dissipation of the spectral multidomain penalty scheme towards resolving the physics of interest.

In this study, an exponential filter [19] is used

$$\sigma(k) = \exp\left[-\alpha\left(\frac{k}{k_c}\right)^p\right], \tag{10}$$

where p is the filter order, k_c represents the index of the highest resolved mode, and $\alpha = -ln(\varepsilon_M)$ with ε_M being the machine precision. The filtered solution u^F may now be expressed in modal form as

$$u^F(z) = \sum_{j=0}^{N} \sigma(k_j)\tilde{u}_j P_j(z), \tag{11}$$

where k_j is the index of the jth Legendre mode and $\tilde{u}_j$ and $P_j(z)$ the corresponding modal coefficients and Legendre polynomials, respectively.

Note that Legendre filters have negligible influence at the subdomain interfaces [19,26], where the influence of the penalty method is the strongest. Thus, the two stabilizing techniques complement each other in enabling numerical stability through the entire extent of a spectral subdomain. Nonetheless, application of Legendre filtering modifies the corresponding

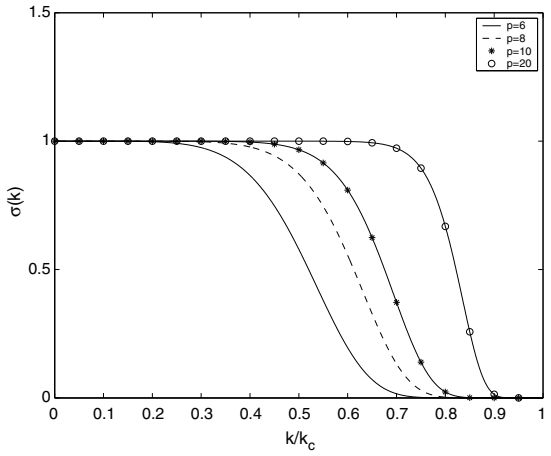

Fig. 2. Exponential filter functions $\sigma(k/k_C)$ for the four different filter orders $p = 6$, 8, 10 and 20 used in this study. In Legendre space, k and k_C represent the mode number and total number of available modes, respectively. In Fourier space, k and k_C represent the two-dimensional wavenumber vector magnitude and the corresponding maximum value over all resolved horizontal wavenumbers, respectively.

modal coefficients and, therefore, violates the patching and boundary conditions [4]. However, unlike the spatially continuous spectral element method [33,2], the inherently discontinuous multidomain penalty scheme is not concerned with preserving the patching and boundary conditions [8]. The error induced by the filtering operation, associated with a small increase in the discontinuity in the solution at the subdomain interface, is minimal and of the same order as the penalty scheme [24]. Nonetheless, this enhancement of interfacial discontinuity by Legendre filtering does bear distinct implications for the behavior of the associated numerical viscosity at the interfaces, as discussed in Section 6.

Expressions analogous to Eqs. (10) and (11) may be constructed for filtering in Fourier space [19]. Note however, that in this study, in Legendre space, k in Eq. (10) represents the kth discrete Legendre mode. In contrast, in Fourier space, for the purpose of implementing efficient two-dimensional filtering, k is elected to represent the magnitude of an individual Fourier wavenumber pair (k_x, k_y), i.e. $k = (k_x^2 + k_y^2)^{1/2}$ and k_c is chosen as $k_c \equiv [(k_{x,\max}^2 + k_{y,\max}^2)]^{1/2}$, i.e. the maximum resolved Fourier wavenumber pair magnitude (for the fields analyzed in this work $k_{x,\max} = k_{y,\max}$). The specific choice of k_c implies that only the top and bottom righthand corners of the solution domain in Fourier space are subject to significant spectral filtering.

In the incompressible spectral multidomain solver presented in this paper, Legendre spectral filtering of the same order p is applied after all three fractional steps in the time discretization summarized in Section 2. Fourier spectral filtering is applied only after advancing the non-linear terms to suppress the accumulation of high-wavenumber numerical driven by aliasing. The specific filters used in this paper are shown in Fig. 2.

4. Simulation description

4.1. Problem geometry

The flow field analyzed in this study is the turbulent wake with non-zero net momentum examined in detail by Diamessis et al. [8,10,11]. Such a flow corresponds to the mid-to-late time wake of a sphere of diameter D towed with a velocity U in a fluid of homogeneous density. Note that the spatial discretization does not account for the sphere and focuses only on the flow generated in its wake. The computational domain of dimensions $L_x \times L_y \times L_z$ is shown in Fig. 3 and corresponds to a window fixed in space with respect to the moving sphere, as do the laboratory measurements [42]. Behind the sphere, the wake is considered to be statistically stationary. The periodicity assumption in the x-direction is valid because the length of the computational domain is much smaller than the total wake length [15]. The spanwise periodicity assumption is also valid provided the horizontal lengthscale of the wake does not become excessively large. The axisymmetric turbulent wake shown schematically in Fig. 3 is a classical example of a free shear flow where turbulence is embedded in a spatially localized mean flow structure. Such a flow configuration provides a convenient framework for the analysis discussed in Section 5. In Fig. 4 we show cross-sections, in the Oxz plane cutting through the wake centerline, of typical vorticity fields from actual simulations at two different Reynolds numbers.

4.2. Initial condition generation

Although the sphere is not accounted for in the computation, its effect must be incorporated in the initial condition. Details of the design of the initial condition and initialization process are given elsewhere [8,11]. The initial flow field is the superposition of an axisymmetric Gaussian mean velocity profile and a turbulent fluctuation field:

$$\mathbf{u}(x,y,z,t) = U_X(y,z,t) + \mathbf{u}'(x,y,z,t). \tag{12}$$

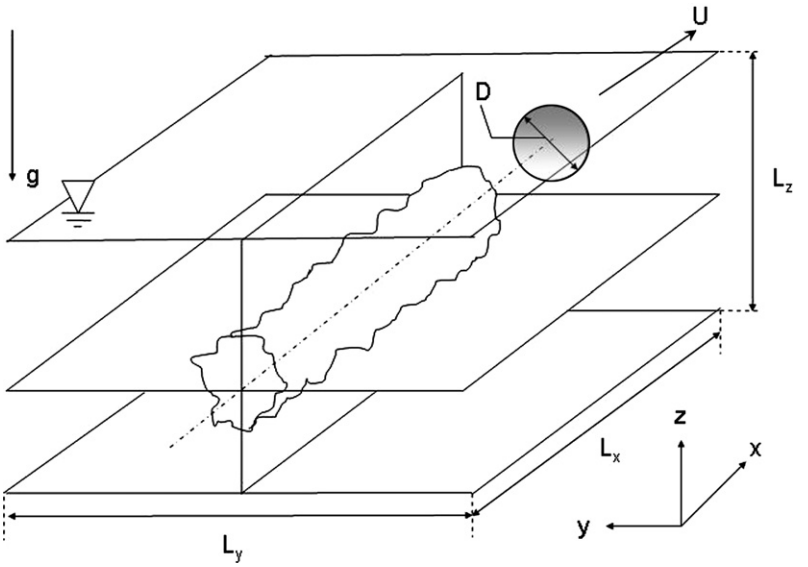

Fig. 3. Computational domain for the simulation of a mid-to-late time turbulent wake with non-zero net momentum. The wake was originally generated by a sphere of diameter D, towed with a velocity U, which however is not present in the computational domain. The domain dimensions are $L_x \times L_y \times L_z$. Consistent with the laboratory water tank the domain has a solid wall bottom and free-slip top. Shown are also the horizontal and vertical centerplane of the flow, the intersection of which determines the wake centerline.

The X subscript indicates averaging in the streamwise direction. Analytical expressions for $U_X(y,z,t)$ and $\mathbf{u}'(x,y,z,t)$ may be found in Diamessis et al. [11]. This initial flow field is constructed to represent a self-similar axisymmetric wake at a distance $x/D = 2$ from the sphere [45,35]. The x-averaged r.m.s. (root mean square) distribution of the fluctuating velocity is assumed to be equipartitioned among its three components. Although laboratory studies on towed sphere wakes [1] indicate self-similarity is first established at $x/D = 6$, the focus of the simulations at hand is to characterize the dynamics of mid-to-late time wake, which should evolve independently of any assumptions about the near-wake flow field, especially given the extensive efforts in designing a robust initial condition [11].

The initial velocity fields of all simulations considered here are the same regardless of Re value. The three-dimensional fluctuating velocity field is constructed as spectrally random noise in three-dimensional Fourier space with a $k^{-5/3}$ energy spectrum. This random field is inverse Fourier transformed and then windowed onto the envelope of the r.m.s. profile of the turbulent fluctuations. Initially, the fluctuating and mean velocity fields are uncorrelated. Thus, a preliminary "relaxation" simulation [15] is run to generate a physically realistic velocity field. During relaxation, the flow is forced to maintain fixed the initially prescribed mean and r.m.s. fluctuating velocity profiles, while the spatial distribution of the turbulent fluctuations, and thus the Reynolds stresses, is allowed to vary. Relaxation is terminated when turbulent production and dissipation reach a steady state.

4.3. Numerical simulations

The purpose of this study is to provide a basic perspective on the effective numerical viscosity embedded in spectral multidomain penalty method models of incompressible flow. Thus, this paper considers only two of the turbulent wake simulations performed in [11], specifically those corresponding to an unstratified fluid at two different values of Re, $Re = UD/\nu = 5 \times 10^3$ and 10^5. U and D are the tow velocity and diameter of the virtual sphere which would produce a turbulent wake whose mean and fluctuating velocity profiles at $x/D = 2$ are used as an initial condition for the simulations examined here. It is emphasized that the Reynolds number is varied by changing the value of ν, i.e. the $Re = 10^5$ run uses a molecular viscosity twenty times weaker than that employed at $Re = 5 \times 10^3$.

The computational domain has a horizontal dimension of $L_x \times L_y = 26\frac{2}{3}D \times 13\frac{1}{3}D$ and corresponds to a virtual stratified water tank of height $L_z = 12D$. A uniform spatial grid is used in the horizontal direction whereas in the vertical the spectral multidomain discretization of Fig. 1 is employed. $M = 7$ and 13 non-uniform height subdomains of order of approximation $N = 24$ and $N = 40$ are used in the vertical direction at $Re = UD/\nu = 5 \times 10^3$ and 10^5, respectively. The positioning of the subdomains is dictated by the requirement of adequate resolution of the energetic scales of the turbulence in the active regions of the flow, which are known a priori. Increased resolution is available at the energetic core of the wake whereas less is utilized in the less active ambient.

The resolution at $Re = 5 \times 10^3$ and 10^5 is $256 \times 128 \times 175$ and $512 \times 256 \times 531$ mesh points, respectively. Fourier and Legendre spectral filters of orders $(p_F, p_L) = (20, 8)$ and (10,6) are used in the low and high Re runs, respectively. Another

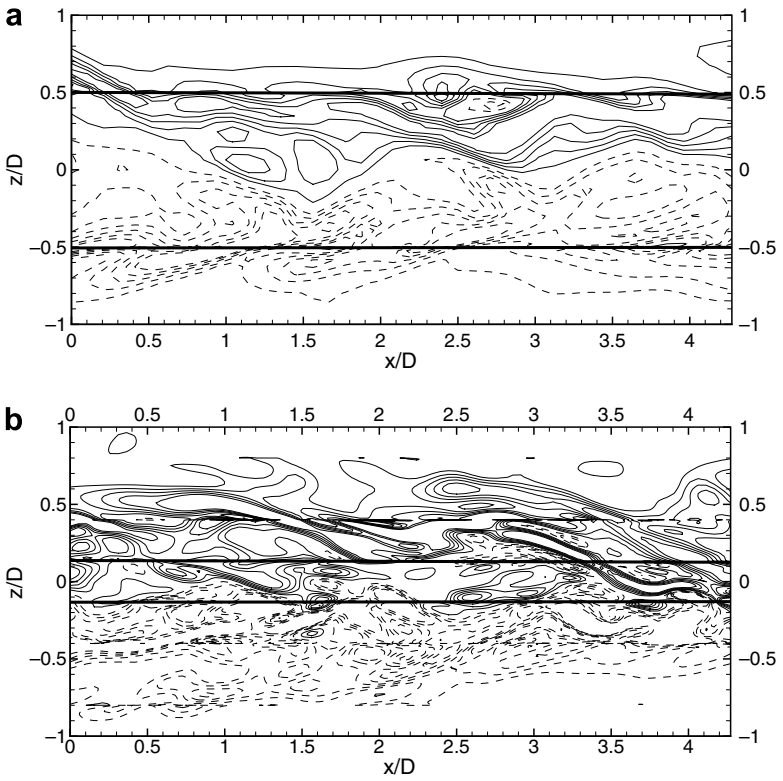

Fig. 4. Contours of spanwise vorticity, ω_y for the simulated turbulent wake of a towed sphere at time $t = 0$ (five timesteps removed from the completion of the relaxation procedure). Shown is an exploded view of data sampled at the Oxz centerplane. (a) $Re = 5 \times 10^3$ and (b) $Re = 10^5$. The min/max contour values are set to $\pm(|\omega_y^{\min}| + |\omega_y^{\max}|)/2$. Solid and dashed lines represent positive and negative values of ω_y, respectively. The horizontal solid lines indicate the interfaces of the central subdomain where the numerical viscosity analysis is performed.

simulation for $Re = 5 \times 10^3$ was performed with resolution $128 \times 64 \times 119$ (corresponding to $M = 7$ subdomains of $N = 16$) and filter orders $(p_F, p_L) = (12, 6)$. Computed one-dimensional Fourier spectra and timeseries of wake lengthscales and velocities exhibited negligible differences with their higher resolution counterparts [11]. In the lower Re case, we have elected to focus our analysis on the higher resolution simulations which capture the physics of the wake core in greater detail without, however, generating any concern about slow run turnaround time. In the higher Re case, resolution is further increased to adequately capture the now even finer energetic scales of motion but also to ensure numerical stability. It is the highest resolution permitted by the available computational resources. At both $Re = 5 \times 10^3$ and 10^5, the values of (p_F, p_L) are chosen to enable a numerically stable solution over long-time integrations, without excessively smoothing out any of the physically significant finer-scale features of the flow fields. Given that, despite the increase in resolution, the $Re = 10^5$ case exhibits a higher degree of under-resolution with respect to its low Re counterpart, a reduction in filter orders is necessary to maintain numerical stability. Finally, the computational timestep Δt is chosen as such that the CFL stability criterion be obeyed in all three spatial directions for a third-order stiffly stable scheme [8].

One-dimensional spectra of turbulent kinetic energy, obtained at the horizontal wake centerplane and averaged over the width of the wake, exhibited no signs of artificial energy accumulation over the range of scales directly affected by the filter. The same features were observed in corresponding two-dimensional spectra (Fig. 5). Similar observations were made for one-dimensional Legendre spectra obtained in the wake core. Thus, the resolutions and filter orders used at each Re are clearly adequate in terms of suppressing Gibbs-oscillations compounded by aliasing at the highest modes of the numerical solution.

All simulations performed employ a MPI-based parallel solver which scales linearly up to 512 processors on a distributed memory cluster [11]. The assignment of different sections of the computational domain to individual processors is based on a one-dimensional domain decomposition which partitions the domain in distinct vertical slabs of thickness L_x/N_P (L_y/N_P) when operating in physical (Fourier) space, where N_P is the number of processors. Three-dimensional velocity fields are outputted at prescribed times. A separate postprocessing code is then used to perform the analysis discussed in Section 5. The $Re = 5 \times 10^3$ runs use $N_P = 32$ processors, whereas their $Re = 10^5$ counterparts require $N_P = 256$. All simulations and postprocessing were performed at the University of Southern California High Performance Computing Center's Linux cluster. On this machine, the average wall-clock time required for a computational timestep is 5 s and 14 s for the low and high Re values, respectively. Note that the respective durations of the "relaxation" runs in wall-clock time were 15 h and 9 days. Given

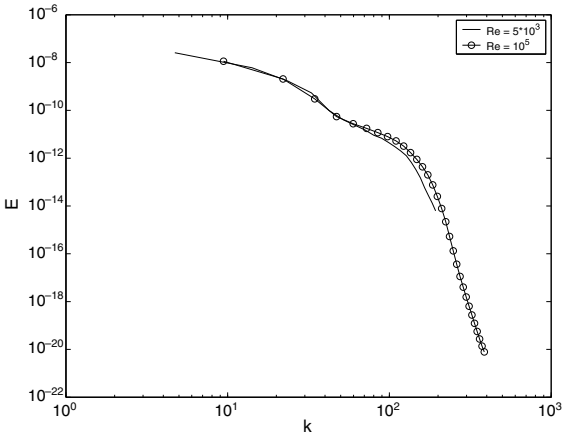

Fig. 5. Two dimensional energy spectra computed at the centerplane ($z = L_z/2$) at the initial time.

our available computational resources, any additional runs at the higher *Re* limit where number of subdomains, subdomain order of approximation and filter order could be varied would be prohibitively costly.

4.4. Choice of initial condition specific to numerical viscosity analysis

The flows that will be analyzed represent a localized turbulent event under the effect of a background shear flow. It is desired that the flow fields are associated with the *most energetic stage* of flow evolution, i.e. the near wake. At this point in flow evolution, the degree of under-resolution is at its maximum, as the scale separation in the turbulent wake, i.e. the separation between the peak in the kinetic energy spectrum and the high-wavenumber motions directly impacted by molecular viscosity (a means of suppressing aliasing-induced effects), is at its largest. As a result and as dictated by experience, the capacity of the spectral filters and penalty schemes to maintain numerical stability is challenged the most at this time. Thus, the near-wake flow fields represent "the worst case scenario" and are the most suitable for evaluating the effective numerical viscosity.

In the same vein, it should also be noted that the propensity for numerical instability in a non-stabilized simulation was found to not depend significantly on the energy content of the higher wavenumber range. Thus, the similarity between the initial two-dimensional spectra in Fig. 5, which suggests the absence of an inertial range in the high *Re* simulations, should not be a cause for concern. The initial one-dimensional streamwise spectra at both *Re* also display the similarity observed in Fig. 5. As discussed in Diamessis et al. [8] (see their Fig. 3 and relevant discussion), the similarity between initial spectra across different *Re* is an artefact of relaxation and does not persist for more than a fraction of an eddy turnover time. Beyond this point, visible differences are rapidly observed across the $Re = 10^5$ and $Re = 5 \times 10^3$ cases. At a time which corresponds to approximately one eddy turnover time after the termination of relaxation, $Re = 10^5$ spectra are found to exhibit a near-decade wide inertial range whereas the equivalent $Re = 5 \times 10^3$ spectra show a much sharper drop-off (not shown here). In summary, the propensity for numerical instability is proportional to the energy content and scale separation in the *physical incarnation* of the turbulent wake. The reduced energy content of the higher resolved wavenumber in the *numerical approximation* of the near-wake is rapidly replenished after the relaxation process is "turned-off".

Beyond being a reliable surrogate of the near-wake, the initial condition for the analyzed datasets is chosen to be immediately after (or nearly so) after the termination of relaxation for two additional reasons: on one hand, this is the initial condition used in stratified wake simulations by the first and third author [10,11] and by others (who employed on low-order finite difference schemes) [15]. An assessment of the effective eddy viscosity in the spectral multidomain penalty scheme would enable an even more rigorous comparison of the former and latter sets of simulations. On the other hand, both *Re* considered here have initial conditions with a comparable spectral signature which allows a clearer assessment of the role of *Re* (and associated choices of resolution and filter orders) on the generated numerical viscosity. Spectra computed at subsequent times in wake evolution do not only exhibit a visible difference at intermediate-to-high wavenumbers across *Re* (due to the emergence of an inertial range at $Re = 10^5$) but also are non-negligibly different at the lower wavenumbers, behavior which would further complicate the analysis and is outside the scope of this paper.

The only concern about the "relaxation" procedure is that it is associated with an artificial input of energy into the flow field by keeping the mean and fluctuating velocity profiles fixed in time. Such artificial energy input could spuriously bias any estimates of energy dissipation required to compute the necessary effective numerical viscosities. Thus, a new initial condition, specifically for the needs of this study, is generated simply by advancing the final state at the end of the "relaxation" by several timesteps, during which the mean and fluctuating profiles are no longer held fixed and may evolve freely. This modified initial condition is the one used for the simulations described in this paper. Specifically, a number of

Table 1
Summary of acronyms of all simulations analyzed in this paper

Run name	Fourier filter	Legendre filter	Penalty method
Total	Yes	Yes	Yes
Fourier	Yes	No	No
Legendre	No	Yes	No
Penalty	No	No	Yes

The acronym of each run indicates what stabilization techniques are used by the numerical method. In the manuscript, the case indicated as "Total" in this table, is also referred to as "fully dissipative". As indicated in Section 5, an additional run used as the non-dissipative baseline is also analyzed, which employs only a $p_L = 20$ and $p_L = 10$ filter in Legendre space for $Re = 5 \times 10^3$ and 10^5, respectively.

simulations are performed at both Reynolds numbers, during which all or only one of the stabilizing techniques described in Section 3 are implemented to better identify the individual contribution of each stabilization method to the effective numerical viscosity of the spectral multidomain penalty scheme. The acronyms used for all simulations are listed in Table 1. In addition to the four runs listed in the table, a nominally non-dissipative baseline case is also considered, which is discussed in more detail in Section 5.

5. Numerical dissipation and effective numerical viscosities

The essence of the method to extract information about implicit numerical dissipation for a particular numerical code is a comparison between the kinetic energy decay rate given by the code in question and the decay rate computed with expressions that minimize or entirely remove effects of the numerical dissipation, symbolically

$$\varepsilon_n = \left[\frac{\partial E}{\partial t}\right]^{\text{nondiss}} - \left[\frac{\partial E}{\partial t}\right]^{\text{diss}}. \tag{13}$$

In application to homogeneous turbulence Domaradzki et al. [13,14] calculated the first term in (13) using pseudo-spectral evaluation of non-linear and viscous terms in the Navier–Stokes equation. The numerical dissipation is then simply a residual of the energy decay rate computed from the dissipative code (the second term) and the combined spectral energy transfer and viscous dissipation terms computed using pseudo-spectral method without numerical dissipation errors.

For inhomogeneous flows a computation of the non-linear and viscous term without numerical dissipation is not that straightforward and a different, and more general, approach is used. The first term in (13) is computed exactly the same way as the second term but using modification of the same code, or entirely different code, that removes or significantly minimizes effects of the numerical dissipation. The same initial condition as for the second term and the same mesh must be employed but the timestep can be decreased to minimize time stepping errors. The primary requirement for such a *nominally* non-dissipative code, in a sense of minimized numerical dissipation, is that it should conserve the total kinetic energy when run in the inviscid mode. Since the energy decay rate can be estimated from data from just two timesteps, such a nominally non-dissipative code will never be run for more than just few timesteps for the purposes of our analysis. Therefore, it does not need to be stable in the long time runs as long as it allows to compute the energy decay rate for a velocity field at a given time without numerical dissipation effects. One can thus visualize the procedure where the actual code is run, producing velocity fields contaminated by the numerical dissipation, and whenever the value of the numerical dissipation is sought, an auxiliary short time simulation is performed with the nominally non-dissipative code.

In the case considered here, numerical dissipation originates from the Legendre spatial discretization, fully implicit time discretization for the viscous term and, most dominantly, the application of stabilizing filters and the penalty method. Note that the artificial dissipation of Legendre/Chebyshev schemes decreases exponentially with increasing N, whereas Fourier discretizations are free of any artificial dissipation (see Section 1 and Ref. [5]). In terms of temporal discretization, through repeated numerical experiments, we have found that the numerical dissipation induced by the combination of a fully implicit scheme with third-order backward differentiation exceeds negligibly that associated with a Crank–Nicholson scheme for the viscous term. We are thus led to conclude that the spectral filters and the penalty method are the main contributors to numerical dissipation.

The natural choice of a *nominally* non-dissipative case would be a simulation where no stabilizer is turned-on. As discussed above, such a baseline non-dissipative code should also *conserve* the total kinetic energy when run in the inviscid mode. In the under-resolved triply-periodic simulations which use Fourier discretization in all three directions, such a simulation is feasible because, in the absence of explicit external forcing, there is no mechanism to inject additional energy into the flow field. However, non-linearity-induced aliasing rapidly intensifies the Gibbs oscillations that develop at the boundaries and subdomain interfaces of non-stabilized under-resolved spectral multidomain simulations (see also Section 2) and produces an increase in the total kinetic energy of the flow. Thus, for the purpose of damping these spurious oscillations, the baseline case in this study consists of a simulation where all stabilizers are turned off except for $p_L = 20$ and $p_L = 10$ Legendre filters for $Re = 5 \times 10^3$ and $Re = 10^5$, respectively. These values of p_L are markedly larger than the corresponding ones used in the fully stabilized simulations and simply serve to produce a simulation that is stable over the time interval that

our effective numerical viscosity analysis is applied. At both *Re*, the nominally non-dissipative case can be run for several timesteps (of O(100)) before becoming unstable (this is of course the reason why in actual, long-time, simulations stronger filters must be used to control numerical instabilities). As discussed above, such short run times are more than sufficient because an auxiliary simulation results are needed only to provide the "non-dissipative" time derivative in Eq. (13) and that can be computed numerically from the fields at only few contiguous timesteps.

For both *Re*, all simulations required for the analysis of the numerical viscosity were run for eight timesteps with a constant value of Δt set by the associated CFL restrictions. Note that numerical tests showed that running with one-half and one-quarter the timestep did not produce a significantly different time stepping error.

Fig. 6a and b shows the decay of the total kinetic energy obtained using the baseline code that minimizes numerical dissipation, i.e., the code that uses only $p_L = 20$ and $p_L = 10$ Legendre filters for $Re = 5 \times 10^3$ and $Re = 10^5$, respectively. In each case shown in Fig. 6a and b the simulations were run for eight timesteps with different values of the molecular viscosity. In particular, in Fig. 6a the kinetic energy decay is shown for the molecular viscosity $\nu = \nu_0$ used in the actual simulations as well as for two more values corresponding to a variation of the above viscosity value by a factor of 10 and 0.1. The baseline cases for $\nu = \nu_0$ for both *Re* are used to calculate the non-dissipative term in Eq. (13). The cases with $\nu = 0.1\nu_0$ approximate the vanishing viscosity limit in which the kinetic energy of a flow should be globally conserved. Indeed, for these cases and for the time intervals considered, it is seen in Fig. 6a that the kinetic energy remains practically constant, satisfying the requirement that the baseline code minimizes the numerical dissipation.

The approach of varying the molecular viscosity in a baseline code with minimized numerical dissipation is also useful in estimating the global numerical viscosity acting over short time intervals in the actual simulations. In Fig. 6b we plot the total energy decay obtained using the full numerical code with all stabilizers turned on (solid lines) and the energy decay obtained using the baseline simulation for different values of the molecular viscosity ν (symbols). The baseline case for

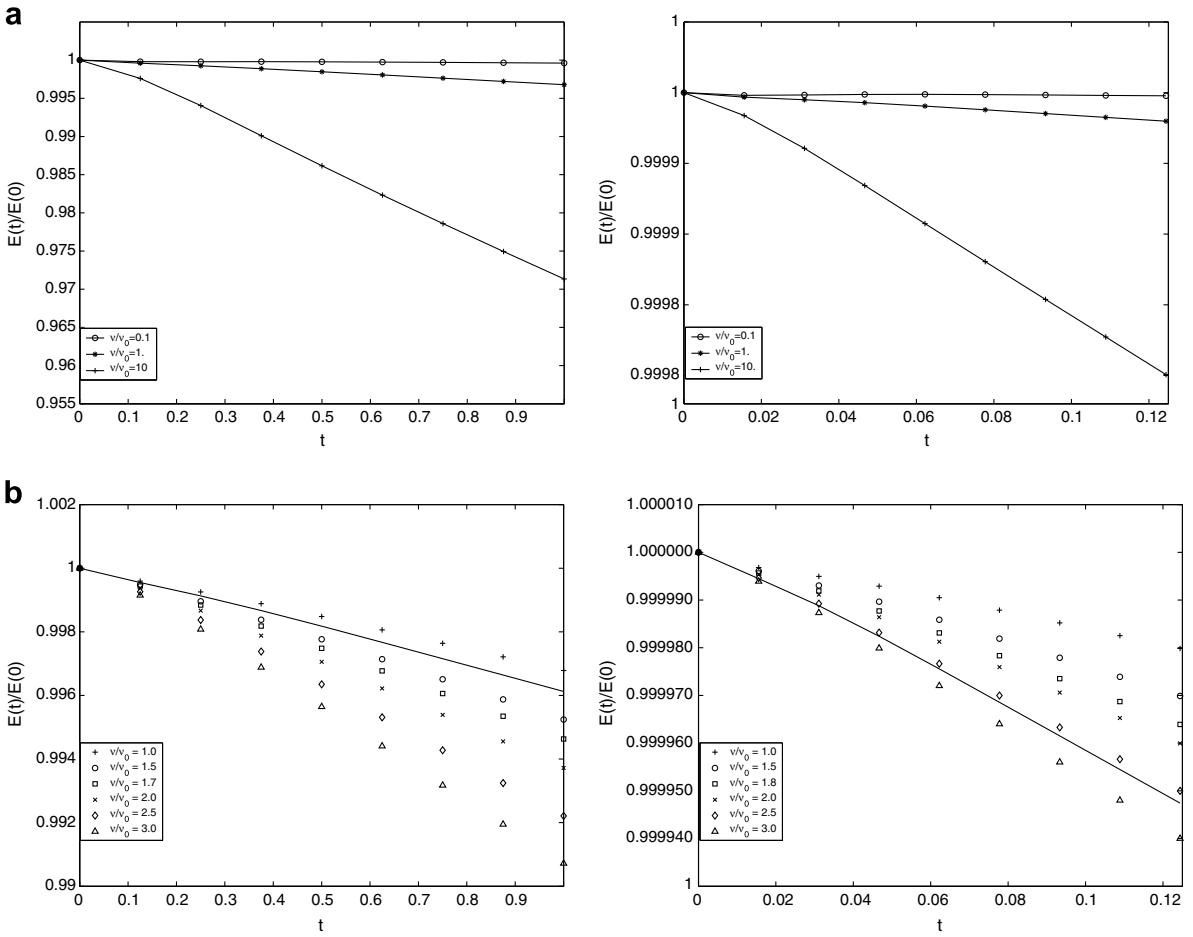

Fig. 6. Decay of total kinetic energy of the flow over the course of eight timesteps for different values of molecular viscosity for the baseline case (i.e. only a weak Legendre filter is turned on). The value of viscosity used in the actual simulations (to obtain the prescribed *Re* value) is denoted by ν_0. Left: $Re = 5 \times 10^3$; Right: $Re = 10^5$. (a) Variation of ν by an order of magnitude and (b) variation by a factor of three or less, with the solid line representing the actual simulation where all stabilizers are turned on.

$\nu \approx 1.25\nu_0$, where ν_0 is the molecular viscosity in the actual simulations, provides the best match to the actual energy decay for the case $Re = 5 \times 10^3$. At $Re = 10^5$ the best match is observed for $\nu \approx 2.5\nu_0$. Therefore, to get the same energy decay, simulations with stabilizers absent (or minimized) require a molecular viscosity that is larger by 25–150% than the value employed in simulations that use stabilizers. This indicates that, depending on *Re*, the numerical dissipation effects can be as significant as the dissipation effects due to the physical viscosity ν_0.

For a simulation at a given *Re*, the ratio ν/ν_0 should clearly decrease towards unity as the simulation becomes increasing well-resolved (a mounting challenge as *Re* is increased) as a broader range of scales would be captured thereby allowing molecular viscosity to have a stronger direct influence over the resolved scales. An increase n in filter order would then be possible, whereas the penalty terms will automatically diminish their contribution automatically as a function of subdomain thickness or order of polynomial approximation *N* [24]. Thus, a decrease in global numerical viscosity, as quantified by the approach outlined above, would be expected. Now, if resolution is kept fixed and *Re* is increased, the penalty terms will strengthen their contribution but, most importantly, a reduction in filter order would be needed for a robust long-time computation. The result would be an increase in global numerical viscosity. Further support towards these conjectures regarding the dependence of numerical viscosity on resolution and *Re* is provided by the model discussed in Section 6.

The global numerical viscosity effects estimated above do not provide information about scale dependence of numerical effects. The scale dependence can be obtained by considering the wave number dependent eddy viscosity, defined for a triply periodic domains in [13,14]. For a flow between two horizontal planes with linear dimensions L_x and L_y in periodic directions x and y, respectively, and a non-periodic z-direction we adopt the following approach.

The kinetic energy balance for various wall-bounded flows is well documented in the classical textbooks on turbulence [36,46,28]. Fourier decomposition of the velocity field in horizontal directions provides information about contributions that various lateral scales of motion, associated with different horizontal wavenumbers, make to the dynamics of the flow. In what follows we will consider a mixed Fourier-physical space representation for any dependent variable $q(\mathbf{x}, t)$ $(= p, u, v, w)$. If values of q are provided on Fourier collocation points $x_m = mL_x/N_x$, $y_n = nL_y/N_y$, where $m = 0, 1, \ldots, N_x$ and $n = 0, 1, \ldots, N_y$, then a discrete inverse Fourier transform with respect to x and y is

$$\mathscr{F}[q](k_x, k_y, z, t) = \frac{1}{N_x N_y} \sum_{m=0}^{N_x-1} \sum_{n=0}^{N_y-1} q(x_m, y_n, z, t) \mathrm{e}^{-\mathrm{i}k_x x_m} \mathrm{e}^{-\mathrm{i}k_y y_n}, \tag{14}$$

where $k_x = 2\pi j/L_x$ and $k_y = 2\pi l/L_y$ with j and l satisfying conditions $-N_x/2 \leqslant j \leqslant N_x/2 - 1$ and $-N_y/2 \leqslant l \leqslant N_y/2 - 1$, respectively.

In this representation the Navier–Stokes equation (1) is written as

$$\frac{\partial}{\partial t} u_n(\mathbf{k}, z, t) = N_n(\mathbf{k}, z, t) + \nu \left(\frac{\partial^2}{\partial z^2} - |k|^2 \right) u_n(\mathbf{k}, z, t) + F_n(\mathbf{k}, z, t), \tag{15}$$

where the index notation is employed, $\mathbf{k} = (k_x, k_y)$, $|k|^2 \doteq k^2 = k_x^2 + k_y^2$, and N_n incorporates all non-linear terms, i.e. it is the sum of the advective and the pressure terms. Also, in what follows we use the same notation for a Fourier transform as for the transformed function if this does not lead to confusion. In numerical simulations performed in the geometry considered here the value of a physical quantity $q(\mathbf{k}, z)$ for $\mathbf{k} = 0$ is equal to a plane averaged mean $\bar{q}(z)$ (Eq. (14)) in the physical space while all modes $\mathbf{k} \neq 0$ constitute fluctuations $q\prime$ about this mean. For this reason the zero mode can be identified with the mean while all non-zero modes can be identified with turbulence.

One easily obtains the equation for the energy amplitude of the mode $\mathbf{k}$

$$E(\mathbf{k}, z) = \frac{1}{2} u_n(\mathbf{k}, z) u_n^*(\mathbf{k}, z), \tag{16}$$

using (15)

$$\frac{\partial}{\partial t} E(\mathbf{k}, z) = \mathscr{R}e[u_n^*(\mathbf{k}, z) F_n(\mathbf{k}, z)] + \mathscr{R}e[u_n^*(\mathbf{k}, z) N_n(\mathbf{k}, z)] + \nu \frac{\partial^2}{\partial z^2} E(\mathbf{k}, z) - 2\nu |k|^2 E(\mathbf{k}, z) - \nu \left(\frac{\partial}{\partial z} u_n(\mathbf{k}, z) \right) \left(\frac{\partial}{\partial z} u_n^*(\mathbf{k}, z) \right), \tag{17}$$

where the asterisk signifies complex conjugate and the summation convention is assumed. Here and in subsequent formulas explicit time dependence is omitted. Terms on the right-hand side of Eq. (17), in the order of occurrence, describe the following physical processes: energy production, energy redistribution by non-linear interactions, redistribution by viscous stresses, dissipation caused by the horizontal gradients of the velocity field, and dissipation attributable to the vertical gradients.

All terms in (17) are scalars which depend on z and have a lateral scale dependence through a two-dimensional wavenumber (k_x, k_y). It is more convenient to work with a single scale-dependent parameter. For turbulence statistically homogeneous and isotropic in the horizontal planes a natural scale-dependent parameter is a wavenumber length $|k| = (k_x^2 + k_y^2)^{1/2}$. For any quantity $q(k_x, k_y, z)$ the dependence on this variable is introduced by summing all modes in circular shells with a prescribed thickness Δk centered at $|k|$:

$$q(k, z) = \sum_{|k| - \frac{1}{2}\Delta k \leqslant |\mathbf{k}| < |k| + \frac{1}{2}\Delta k} q(\mathbf{k}, z). \tag{18}$$

While our fields are not isotropic in horizontal planes, we still will use shell averaging as the simplest mechanism for obtaining scale dependent quantities. For instance, the energy spectra obtained from the numerical simulations at the horizontal centerplane of the flow as a function of horizontal wavenumber k are shown in Fig. 5.

Consider now a numerical simulation performed with a full Navier–Stokes solver and a timestep Δt. For a velocity field $u_i(\mathbf{x}, t)$, obtained in the simulation at time t, the energy spectrum $E(k, z, t)$ can be computed using discrete Fourier transforms and Eqs. (16) and (18). The energy decay rate is computed from such data using backward finite differences

$$\frac{\partial}{\partial t}E(k,z,t) \approx \frac{\gamma_0 E(k,z,t+\Delta t) - \sum_{i=0}^{2}\alpha_i E(k,z,t-i\Delta t)}{\Delta t} \tag{19}$$

and for sufficiently small timestep is an accurate approximation to the decay rate defined by Eq. (17). The coefficients γ_0 and α_i ($i = 0, 1, 2$) for third backward differentiation may be found in Karniadakis et al. [30]. The difference between decay rates computed using velocity fields from the actual solver and the baseline 'pseudo-inviscid' solver provides a k-dependent numerical dissipation

$$\varepsilon_n(k,z) = \left[\frac{\partial E(k,z)}{\partial t}\right]^{\text{nondiss}} - \left[\frac{\partial E(k,z)}{\partial t}\right]^{\text{diss}}, \tag{20}$$

where the first and second terms on the right-hand side represent, respectively the energy decay rate for the baseline case and the specific case under consideration, with all or one of the stabilizers turned on (see Table 1).

In the theory of homogeneous, isotropic turbulence, a wavenumber dependent subgrid scale dissipation can be used to define a wavenumber-dependent eddy viscosity, as was first proposed by Kraichnan [31]. The definition

$$\nu_{\text{SGS}}(k) = \frac{\varepsilon_{\text{SGS}}(k)}{2k^2E(k)}, \tag{21}$$

where $E(k)$ is the three-dimensional energy spectrum and $\varepsilon_{\text{SGS}}(k)$ is the energy loss at scale k due to subgrid scale interactions, is based on the analogy with the exact expression for the viscous dissipation

$$\varepsilon_\nu(k) = 2\nu k^2 E(k). \tag{22}$$

The same analogy has been used in defining a numerical viscosity acting in numerical simulations of isotropic turbulence performed with a finite volume code [48,14]

$$\nu_n(k) = \frac{\varepsilon_n(k)}{2k^2E(k)}. \tag{23}$$

We will use the same formal definition in the current analysis of simulations with one inhomogeneous direction, i.e., we define the k-dependent numerical viscosity for each z-plane as

$$\nu_n(k,z) = \frac{\varepsilon_n(k,z)}{2k^2E(k,z)}. \tag{24}$$

It must be noted, however, that while the definition (23) is unique for isotropic turbulence, forms other than (24) can be considered for inhomogeneous turbulence. Indeed, in the energy Eq. (17) the total viscous dissipation in a plane z is represented by the last two terms on the r.h.s. Therefore, one could also require that the numerical dissipation $\varepsilon_n(k,z)$ be expressed in the form of the last term, proportional to the vertical velocity gradients, or some combination of both terms, e.g.

$$\nu_n(k,z) = \frac{\varepsilon_n(k,z)}{2k^2E(k,z) + \left|\frac{\partial}{\partial z}u(k,z)\right|^2}, \tag{25}$$

where $\left|\frac{\partial}{\partial z}u(k,z)\right|^2$ is $\left(\frac{\partial}{\partial z}u_n(\mathbf{k},z)\right)\left(\frac{\partial}{\partial z}u_n^*(\mathbf{k},z)\right)$ summed over shells according to the definition (18). The choice of (24) simply makes comparisons with previous results for isotropic turbulence easier. It must be stressed, however, that irrespective of the choice, the total numerical dissipation is accounted for because the numerical viscosity (24) is calculated from $\varepsilon_n(k,z)$, Eq. (20). Eq. (24) merely expresses the total numerical dissipation entirely in terms of the horizontal velocity gradients in z-plane (the term $k^2E(k,z)$), with $\nu_n(k,z)$ as the proportionality factor. For completeness, some results for the numerical viscosity computed using both definitions (24) and (25) will be compared.

For the runs listed in Table 1, five choices for the spectrum $E(k,z)$ used in the normalization of the numerical dissipation in Eqs. (24) and (25) are possible: the spectrum obtained in the specific run under consideration (fully dissipative, Fourier, Legendre or Penalty cases) or the equivalent spectrum for the baseline case. In the analysis that follows, we elect to normalize with $E(k,z)$ obtained from the baseline case, as this case provides a common platform for comparison of the numerical dissipation rate as computed for all simulations employing at least one form of stabilizer. This approach is further motivated by the assumption that at each timestep, within the short duration of all runs considered here, the spectra $E(k,z)$ for baseline and fully dissipative cases are not appreciably different. It is only the energy decay rate as a function of wavenumber which exhibits significant differences across runs. Furthermore, it should be emphasized that we are primarily interested in

quantifying the numerical dissipation due to different stabilization techniques. Normalization with $2k^2E(k,z)$ simply enables an efficient comparison of numerical dissipation with the dissipation driven by molecular effects.

6. Results

Results on the effective numerical viscosity of the spectral multidomain penalty scheme are now presented. All results shown here are computed at the fifth timestep of the simulation under consideration. No significant differences were observed at prior or subsequent timesteps. Given that we focus on quantifying the effective numerical viscosity during the most energetic time of flow evolution, our analysis will concentrate on the most energetic spatial region of the flow, i.e. the wake core, and particularly at the center and interfaces of the central subdomain (see Fig. 4).

Fig. 7 shows the numerical eddy viscosity ν_n computed according to Eq. (24) (Fig. 7a) and (25) (Fig. 7b) on the horizontal centerplane (at $z = L_z/2$), i.e., the center of the middle subdomain (see Fig. 4). Computation of ν_n using Eq. (24) or Eq. (25) does not reveal any significant differences over the entire range of resolved wavenumbers. The total numerical viscosity produced when all stabilizers are turned on is dominated by Legendre filtering at large and intermediate scales and Fourier filtering at small scales. Application of only the Fourier filter is accompanied by numerical viscosity that is negligible at small wavenumbers and becomes significant at $k/k_c \geqslant 0.85$ and 0.45 for $Re = 5 \times 10^3$ and 10^5, respectively, where the value of ν_n/ν begins to visibly exceed unity. Although the maximum value of ν_n/ν for the strict application of the Legendre filter is weaker than its Fourier counterpart, the Legendre filter induces a numerical viscosity that is non-negligible over the entire range of wavenumbers. Its peak value is observed at the highest wavenumbers for both Re. For $Re = 5 \times 10^3$, the normalized Legendre-filter-induced numerical viscosity generally does not exceed unity for $k/k_c < 0.85$. If the effective Reynolds number of a simulation is determined using a cumulative effect of the molecular and the numerical viscosity, the Legendre filter does not significantly impact the effective Reynolds number in this case. In contrast, the corresponding normalized viscosity for $Re = 10^5$ remains consistently above a value of one suggesting at least a two-fold reduction of the effective Reynolds number. At the horizontal centerplane, which is also the element centerplane, the penalty method has a negligible effect over all scales because it is designed to ensure stability only in the vicinity of the subdomain interfaces.

The sensitivity to the choice of $E(k,z)$ in the denominator of Eq. (24) is examined in Fig. 7c. For the eight-timestep duration of the $Re = 5 \times 10^3$ runs, the ν_n/ν curves are nearly identical across all wavenumbers for a normalization with $E(k,z)$ from either the baseline or the fully dissipative case. However, *at higher wavenumbers*, i.e. $k/k_c > 0.6$, the ν_n/ν curves at $Re = 10^5$, for the fully dissipative and Fourier-only cases, exhibit a difference of two orders of magnitude for normalization with $E(k,z)$ chosen from either the baseline or the fully dissipative case. In the latter case, a cusp-like maximum is now clearly visible at the largest wavenumber. This sensitivity at high wavenumbers of the higher Re simulations may be attributed to their higher degree of under-resolution (see also the discussion in Section 4.3), which allows the faster contamination of the higher horizontal Fourier wavenumbers with numerical noise originally generated in the vertical direction. Nonetheless, the physical implications of these very large values of numerical viscosity at high values of k/k_c are secondary. The behavior of this range of wavenumbers, whose primary purpose is to ensure numerical stability, is controlled by the spectral filter. The associated energy content is negligible (below machine precision, see Fig. 5) and, therefore, the large values of the numerical viscosity do not impact directly the energy-containing scales. Furthermore, as evidenced by the insert in the right column of Fig. 7c, for $k/k_c < 0.4$ (the range of wavenumbers not directly influenced by the filter), the choice of normalization spectrum has no impact on the value of numerical viscosity.

By appealing to a simplified model 'simulation', the large variation in magnitude of the numerical viscosity at high wavenumbers for the two values of Re may be shown to be primarily due to the application of the Fourier filter. Such a simulation considers an initial velocity field whose energy spectrum on a prescribed horizontal plane at a prescribed vertical location is given by $E_0 = E(k, t = 0)$. The simulation is advanced through the successive application of a Fourier filter of order p_F in both horizontal directions at each timestep. This approach is essentially equivalent to running a three-dimensional simulation of evolution equations for all three velocity components whose right-hand side consists only of p_Fth order hyperviscous operators in the x- and y-directions [4,19]. Successive application of this filter to the initial condition yields, after n timesteps, the energy spectrum:

$$E(n\Delta t) = E_0 \ \exp\left[-2n\alpha\left(\frac{k}{k_c}\right)^{p_F}\right]. \tag{26}$$

Differentiating this equation with respect to time, where $t = n\Delta t$ leads to an energy decay rate:

$$\left[\frac{\partial E}{\partial t}\right]^{\text{diss}} = \frac{E_0}{\Delta t}\left[-2\alpha\left(\frac{k}{k_c}\right)^{p_F}\right]\exp\left[-2n\alpha\left(\frac{k}{k_c}\right)^{p_F}\right]. \tag{27}$$

Note that, in the context of this specific idealized simulation, where Navier–Stokes dynamics are "turned-off", the equivalent non-dissipative baseline case is assumed to produce $[\partial E/\partial t]^{\text{nondiss}} = 0$.

Eq. (27) suggests that the energy decay rate due to the Fourier filter is determined by filter order p_F and timestep Δt. The $-2\alpha(k/k_c)^{p_F}$ term exhibits a maximum at the largest wavenumber. The multiplication of this term by the p_F-order exponential function in Eq. (27) results in a distinct peak whose location will shift to the left with decreasing p_F. Thus, for a given resolution, the numerical dissipation rate will peak at progressively smaller wavenumbers when filter order is reduced, as

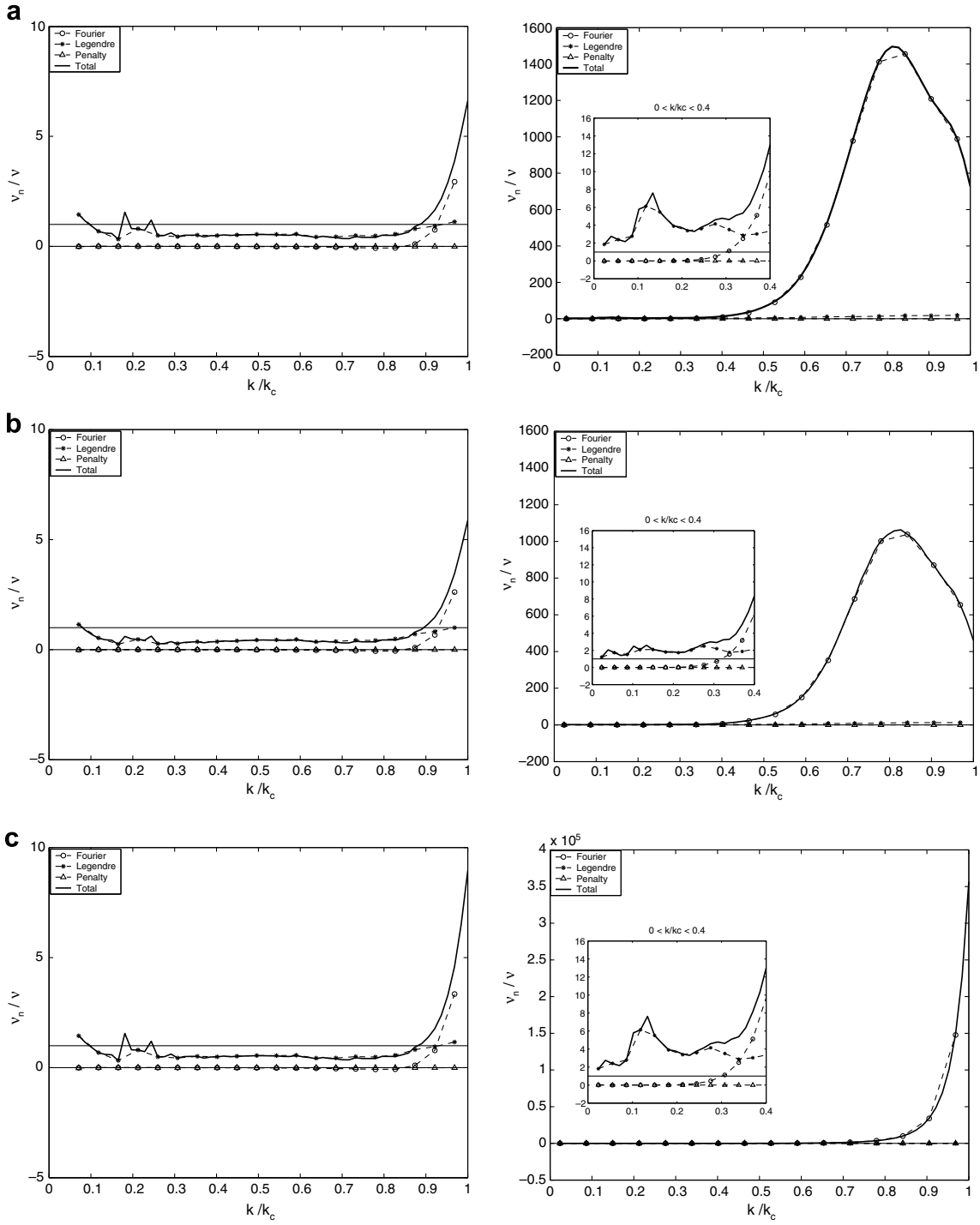

Fig. 7. Effective numerical viscosity (normalized by the molecular viscosity) at the horizontal centerplane of the flow. (a) Eq. (24), normalized with baseline case spectra; (b) Eq. (25), normalized with baseline case spectra. (c) Eq. (24), normalized with fully dissipative case spectra. The horizontal lines indicate values $\nu_n/\nu = 1$. The insert zooms into region $k/k_c < 0.4$. Note the difference in two orders of magnitude in the vertical axis of the right column in (c) compared to (a) and (b).

the filter function impacts an increasingly broader band of higher modes (Fig. 2). Increasing resolution is effectively equal to increasing k_c, which would have the opposite effect: for a fixed value of p_F, the numerical dissipation rate peak would be shifted to larger dimensional values of k, i.e. the lower end of the wavenumber band subject to the direct influence of numerical dissipation would be shifted to higher values. Such an observation can also follow from Fig. 2. As already indicated in

Section 4.3, resolution and filter order are chosen as high as possible within the limits of available computational resources to allow for as broad as possible a range of resolved scales directly unaffected by the action of the spectral filter.

Using as initial conditions those employed in the actual Navier–Stokes simulations, the numerical viscosity for model simulations, computed through Eqs. (24) and (27), is shown for the two *Re* values in Fig. 8. The numerical viscosity is compared to that obtained from a Navier–Stokes simulation using only a Fourier filter as a stabilizer (see Table 1). Normalization of the numerical dissipation rate for both Navier–Stokes and model simulations is performed using the spectrum $E(k,z)$ from the *corresponding baseline case*. For the Fourier-filtered Navier–Stokes simulations the baseline case is the one described in Section 5. However, note that, for a purely analytical model (26) and (27), the normalization of the numerical dissipation is performed using spectrum E_0 since the baseline case associated with the model preserves the initial energy spectrum. Following the discussion of Section 5 and earlier parts of this section, this choice of normalization is responsible for a local, and not cusp-like maximum, at high wavenumbers for $Re = 10^5$. However, if the normalization were done using the evolved spectrum (26) a cusp at the maximum wavenumber would be observed in the analytical model of the numerical viscosity.

In Fig. 8, the order of the filter, $p_F = 20$ and 10 for $Re = 5 \times 10^3$ and $Re = 10^5$, respectively, dominates the form of the numerical viscosity function and is responsible for the left-shifted peak in the higher *Re* case. The normalized numerical viscosity shown in Fig. 8 for $Re = 10^5$ is roughly 200 times larger than its $Re = 5 \times 10^3$ counterpart for two reasons. As indicated in Section 4, the Reynolds number is varied by modifying the physical viscosity, which is a factor of 20 less for the $Re = 10^5$ case. Because the numerical viscosity in Fig. 8 is non-dimensionalized by ν, the plotted values will exhibit a relative increase across *Re* by a factor of 20. Additionally, by means of the CFL condition, the significantly finer grid resolution of the $Re = 10^5$ case requires use of a timestep approximately 1/10 the value of its low *Re* counterpart. An explicit scaling of (27) with the timestep will further increase the plotted values by the inverse of Δt. Thus, a total increase of an approximate factor of 200 in ν_n/ν is observed in the $Re = 10^5$ with respect to their $Re = 5 \times 10^3$ counterparts. Note that the enhancement of ν_n/ν due to smaller Δt at higher *Re* may also be interpreted by considering that the smoothing/dissipative effect of the spectral filter, which is applied at every timestep, acts over a much shorter interval in the higher *Re* case. Running the actual Navier–Stokes solver with the same initial condition and only Fourier-filtering turned on indicates that Navier–Stokes dynamics enhance the numerical viscosity. Such an enhancement is most likely due to the increase of small-scale energy content through nonlinear energy transfer mechanisms from the larger scales in the flow.

The scale-dependent numerical viscosity induced by individual stabilizers (Fourier, Legendre and penalty) and all combinations thereof at the bottom and top interfaces of the central subdomain are plotted in Fig. 9. At both Reynolds numbers, Fourier filtering produces a numerical viscosity that is distributed across wavenumbers in a manner similar to that at the center of the subdomain (Fig. 7). The normalized numerical viscosity is negligible at low wavenumbers and begins to transition above unity at the same value of k/k_c for which the corresponding transition happens at the subdomain center. Clearly, Fourier filtering is the dominant contributor to the numerical viscosity over all wavenumbers at $Re = 10^5$ when all stabilizers are turned on, overpowering the effect of Legendre filtering and the penalty scheme. A similar observation does not hold for the $Re = 5 \times 10^3$ run. In this case, the numerical viscosity at high wavenumbers exhibits negative values, which signify anti-dissipative behavior. These negative values are attributed to the penalty scheme, which, when introduced individually, induces a negative numerical viscosity at high wavenumbers (the negative values for the $Re = 10^5$ case are more visible in the right panel of Fig. 10).

The anti-dissipative behavior of the penalty scheme may initially be regarded as counter-intuitive. The basic premise associated with introducing the penalty terms at subdomain interfaces is that the accompanying penalty terms act to bound the energy of the discrete equations [25]. One would expect any such action to be of strictly dissipative nature. An interpre-

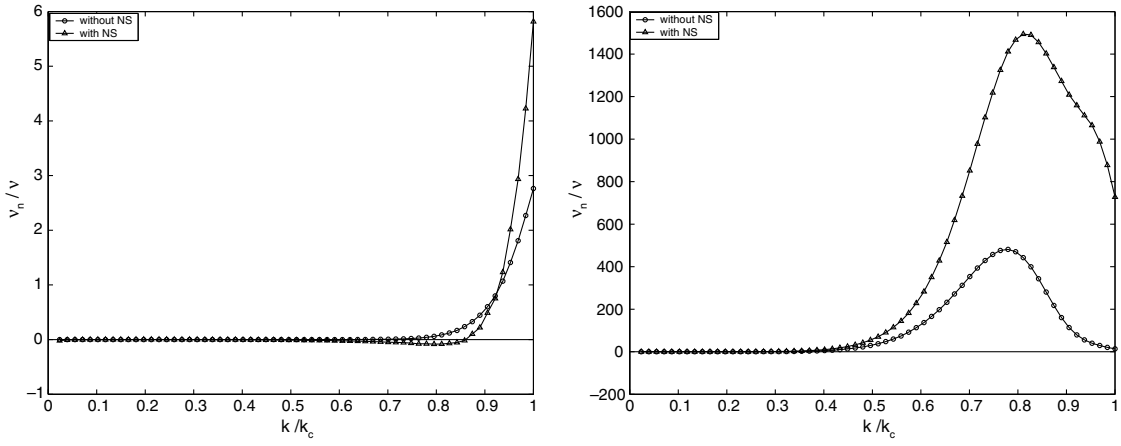

Fig. 8. Comparison of numerical viscosity (normalized by the molecular viscosity) at the horizontal centerplane obtained using a model simulation with only Fourier filtering and a Navier–Stokes simulation with only the Fourier filter turned on (see Table 1) (left: $Re = 5 \times 10^3$; right: $Re = 10^5$).

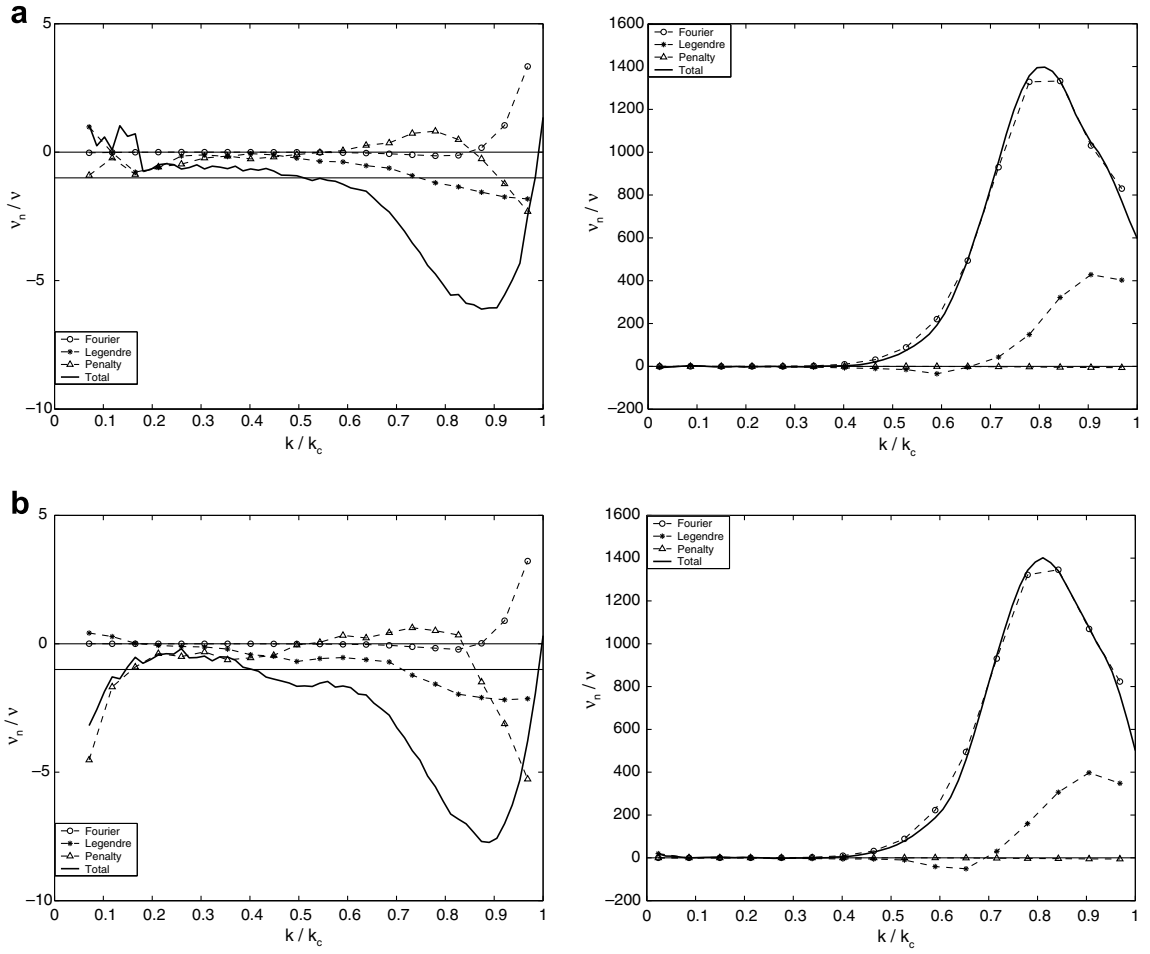

Fig. 9. Effective numerical viscosity (normalized by the molecular viscosity) at the two interfaces of the central computational subdomain of the flow for the different types of simulations described in Table 1. (a) Bottom interface and (b) top interface (left: $Re = 5 \times 10^3$; right: $Re = 10^5$).

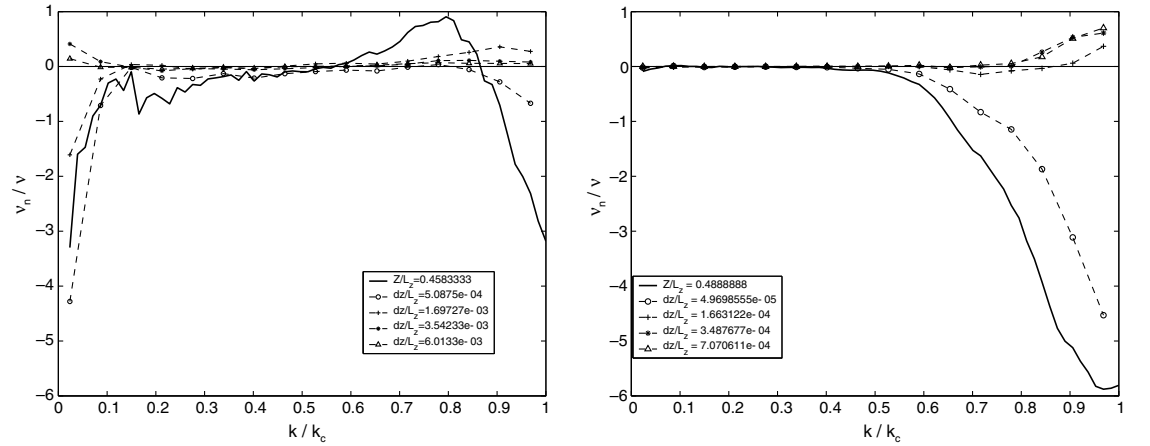

Fig. 10. Comparison of numerical viscosity (normalized by the molecular viscosity) at the central subdomain's bottom interface (located at $Z/L_z = 0.825/1.8$ for $Re = 5 \times 10^3$ and at $Z/L_z = 0.88/1.8$ for $Re = 10^5$) as well as four grid points (the legend showing the distance $dz/L_z = (z - Z)/L_z$ from the interface) above the interface of the central subdomain for simulations with only the penalty method turned-on. (left: $Re = 5 \times 10^3$; right: $Re = 10^5$).

tation for the observed anti-dissipative numerical viscosity at high wavenumbers can be offered by recalling that the incorporation of a penalty term in the governing equations relaxes the solution at the interfaces by satisfying both equations and patching condition, thereby weakly enforcing C_0 continuity at the subdomain interfaces. The resulting weak discontinuity observed at the subdomain interfaces automatically generates a small error which is comparable to the order of the scheme [24]. This weak interfacial discontinuity should lead to an increase of the energy content of the highest Legendre modes as their fine-scale variation becomes most prominent at these locations [5]. Energy transfer through non-linearity of the Navier–Stokes equations to all other spatial directions will then increase the energy content at high Fourier wavenumbers, i.e. lead to the controlled accumulation of "numerical noise". Obviously, this growth in higher Fourier mode energy content does not have an adverse impact on the stability of the long-time integration of the Navier–Stokes equations. Nevertheless, based on the analysis of Section 5, it is manifested as anti-dissipative behavior locally in Fourier space.

Note that Legendre filtering also produces negative values of numerical viscosity at high wavenumbers for $Re = 5 \times 10^3$. Taking into account the discussion of Section 3.2) on violation of patching/boundary conditions by Legendre spectral filtering, this anti-dissipative behavior may be explained with arguments similar to those used for the penalty scheme. Now, the equivalent numerical viscosity for the high *Re* run is distinctly positive with the exception of weakly negative values in the wavenumber band $[k, k_c] \in [0.55, 0.65]$. These distinct differences in the role of Legendre filtering across *Re* and the persistently anti-dissipative behavior of the penalty scheme at both *Re* indicate that further analysis, beyond the scope of this paper, would eventually be needed. Such analysis would identify the numerical viscosity induced by these stabilizers as a function of Legendre mode.

Finally, for the purpose of assessing dependence of the anti-dissipative effects of the penalty scheme (when it is individually applied) as a function of distance from subdomain interfaces, the total numerical viscosity at the bottom interface of the central subdomain, and at four mesh points above it, is shown in Fig. 10. The anti-dissipative effects do not persist more that one point beyond the interface. With increasing distance from the interface, the numerical viscosity exhibits an increasingly weaker positive value. Similar analysis was performed over an additional number of timesteps revealing no significant difference.

7. Conclusions

In this work we have extended the numerical viscosity analysis from homogeneous, isotropic configurations (i.e. triply periodic domains) to doubly periodic domains with one inhomogeneous direction. In principle, the approach signified by Eq. (13), is quite general and can be applied to an arbitrary code as long as an auxiliary "non-dissipative" case can be constructed. The specific numerical code analyzed in this work is based on a spectral multidomain method model stabilized by the application of Fourier and Legendre filters and a penalty scheme. The primary motivation for using the stabilizing techniques is the need to run the simulations at high Reynolds numbers, often two or higher orders of magnitude greater than possible without using stabilizers. The stabilizers are applied selectively, only either at the smallest scales, i.e. for wavenumbers or polynomial orders close to maximum values, or in the immediate vicinity of domain interfaces and boundaries. It is thus expected that scales and the physical regions not explicitly affected by the stabilizers are governed by the Navier–Stokes dynamics and therefore experience only an indirect stabilizer effect. The analyses reported here quantify this expectation in terms of the numerical viscosity that can be attributed to the stabilizers, and which in turn is compared with the molecular viscosity used in the actual simulations. The method is based on a comparison between the kinetic energy evolution given by the analyzed code and a corresponding evolution obtained using a code that minimizes effects of the numerical dissipation. Ideally, such a code would be fully non-dissipative which, however, is not possible in an under-resolved simulation employing an element-based spectral discretization. Thus, the baseline code employs only a very weak Legendre spectral filter which allows it to conserve its energy for a time long enough for the above comparison to be made. The base flow for our investigations are simulations of the turbulent wake of a towed sphere at two different Reynolds numbers, which vary by a factor of 20.

Comparing simulations performed with the stabilizers and with the "non-dissipative" baseline code revealed that the molecular viscosity in the latter case may be a factor 2.5 greater (for $Re = 10^5$) than for the case with the stabilizers in order to match kinetic energy decay rates. This implies that the global numerical viscosity effects are comparable to the effects of the molecular viscosity. This observation also suggests that, as far as the dissipative effects are concerned, the simulations at the highest Reynolds number are not unlike ILES.

When the scale dependence of the numerical viscosity is considered, a qualitatively different behavior is observed in the vicinity of interfaces and away from them. Over a range of high wavenumbers, whose lower end decreases with increasing Reynolds number, the numerical viscosity is dominated by the effect of the Fourier filter. A simple model, based on the evolution of an initial condition through only Fourier filtering in the horizontal, indicates that the peak value of the normalized numerical viscosity scales with Reynolds number and the inverse of the timestep and is located at a wavenumber determined by spectral filter order. Legendre filtering has a relatively weaker contribution to high wavenumbers but is the dominant contributor at lower wavenumbers, producing a numerical viscosity that may be of the order of multiples of the physical viscosity. In the subdomain interiors, the penalty method has negligible effects.

At the interfaces, the penalty method unexpectedly induces a numerical viscosity that is distinctly negative over a significant range of high wavenumbers, i.e., the penalty scheme ensures numerical stability in an anti-dissipative manner. This

anti-dissipative behavior may be explained by the weak enforcement of continuity by the penalty method at the interfaces, which allows for weak discontinuities at these locations. As a result, a minute accumulation of numerical noise, and thus kinetic energy, at the highest Fourier modes could ensue, which nonetheless will not impact detrimentally the long-time integration of the governing equations. At low Reynolds numbers, Legendre filtering produces comparable anti-dissipative behavior which may be explained using similar arguments.

The primary conclusion from the analyses of the numerical viscosity performed here is that the effects of the stabilizers are significant, being comparable, and sometimes larger, than the effects of the physical viscosity. Additionally, while the stabilizers have an expected dissipative character away from the interfaces and boundaries, a strong anti-dissipative character is observed at the interfaces, particularly for the penalty scheme. This observation implies that the stability of the simulations at those locations is achieved not by increasing the artificial dissipation. We believe that relaxing the interface conditions provides the flow variables freedom to adjust without forcing catastrophic Gibbs' oscillations leading to discontinuities in the solution. This freedom and resulting discontinuities are manifested in the form of a negative numerical viscosity.

The findings of this study are only an initial attempt to quantify the effective numerical viscosity in discontinuous high-order multidomain simulations of complex fluid flows. We have restricted ourselves to working with existing simulations at previously specified Reynolds numbers, orders of approximation within each subdomain, filter orders and initial conditions. Beyond the purpose of exactly parameterizing numerical dissipation, it is obvious that for either of the two simulations considered in this paper, reducing the filter order would increase the numerical viscosity. In contrast, increasing the order of approximation in each subdomain or reducing the Reynolds number (by increasing the molecular viscosity) would reduce the degree of under-resolution and thus, clearly decrease the numerical viscosity. Finally, the behavior of numerical dissipation at higher *Re* simulations with an initial condition that exhibits an inertial subrange of at least a decade remains to be determined. For the moment being, we speculate that it may not be dramatically different than that for the initial conditions of the $Re = 10^5$ runs considered here, as it is the degree of under-resolution and not the energy content of intermediate wavenumbers which we find to be the primary cause for numerical instability in the spectral multidomain penalty solver.

Furthermore, significant insight may be obtained by developing an analysis in Legendre space similar to that elaborated upon in Section 5. More conclusive statements could thus be made on the Legendre-filter-induced numerical viscosity as a function of Legendre mode, and particularly about the (anti-)dissipative behavior of this type of filtering and penalty methods at the subdomain interfaces. The design of such an analysis would require the precise definition of energy of the solution as a function of Legendre mode and the formulation of an energy evolution equation in Legendre space. The latter task may be significantly more challenging than in Fourier space due to the more complex properties of Legendre polynomials [5]. We do plan to pursue research in this direction, especially since it can provide a tool that is generalizable to fluid flow simulations in more complex geometries, which utilize two-dimensional quadrilateral or triangular subdomains [39,18,40].

Acknowledgement

The numerical simulations and analysis have been performed the University of Southern California High Performance Computing Center's Linux cluster.

References

[1] P.M. Bevilaqua, P.S. Lykoudis, Turbulence memory in self-preserving wakes, J. Fluid Mech. 89 (1978) 589–606.
[2] H.M. Blackburn, S. Schmidt, Spectral element filtering techniques for large eddy simulation with dynamic estimation, J. Comp. Phys. 186 (2003) 610–629.
[3] J.P. Boris, F.F. Grinstein, E.S. Oran, R.L. Kolbe, New insights into large eddy simulation, Fluid Dyn. Res. 10 (1992) 199–228.
[4] J.P. Boyd, Two comments on filtering (artificial viscosity) for Chebyshev and Legendre spectral and spectral element methods: preserving boundary conditions and interpretation of the filter as a diffusion, J. Comp. Phys. 143 (1998) 283–288.
[5] J.P. Boyd, Chebyshev and Fourier Spectral Methods, Dover, Mineola, New York, 2001.
[6] A.W. Cook, W.H. Cabot, Hyperviscosity for shock-turbulence interactions, J. Comp. Phys. 203 (2005) 379–385.
[7] M.O. Deville, P.F. Fischer, E.H. Mund, High Order Methods for Incompressible Fluid Flow, Cambridge University Press, 2002.
[8] P.J. Diamessis, J.A. Domaradzki, J.S. Hesthaven, A spectral multidomain penalty method model for the simulation of high Reynolds number localized stratified turbulence, J. Comp. Phys. 202 (2005) 298–322.
[9] P.J. Diamessis, L.G. Redekopp, Numerical investigation of solitary internal wave-induced global instability in shallow water benthic boundary layers, J. Phys. Oceanogr. 36 (5) (2006) 784–812.
[10] P.J. Diamessis, G.R. Spedding, Scaling and structure of stratified turbulent wakes at high Reynolds numbers, in: Stratified Flows – Sixth International Symposium, Perth, Australia, 2006, pp. 183–188.
[11] P.J. Diamessis, G.R. Spedding, J.A. Domaradzki, Similarity scaling and vorticity structure in high Reynolds number stably stratified turbulent wakes. J. Fluid Mech. (in preparation).
[12] J.A. Domaradzki, N.A. Adams, Direct modelling of subgrid scales of turbulence in large eddy simulations, J. Turbulence 3 (2002) 1–19.
[13] J.A. Domaradzki, Z. Xiao, P.K. Smolarkiewicz, Effective eddy viscosities in implicit large eddy simulations of turbulent flows, Phys. Fluids 15 (2003) 3890–3893.
[14] J.A. Domaradzki, S. Radhakrishnan, Effective eddy viscosities in implicit modeling of decaying high Reynolds number turbulence with and without rotation, Fluid Dyn. Res. 36 (2005) 385–406.
[15] D.G. Dommermuth, J.W. Rottman, G.E. Innis, E.A. Novikov, Numerical simulation of the wake of a towed sphere in a weakly stratified fluid, J. Fluid Mech. 473 (2002) 83–101.
[16] W.S. Don, D. Gottlieb, J.H. Jung, A multidomain spectral method for supersonic reactive flows, J. Comp. Phys. 192 (2003) 325–354.
[17] F.X. Giraldo, J.S. Hesthaven, T. Warburton, Nodal high-order discontinuous Galerkin methods for the spherical shallow water equations, J. Comp. Phys. 181 (2002) 499–525.

[18] F.X. Giraldo, M. Restelli, A study of spectral element and discontinuous Galerkin methods for mesoscale atmospheric modeling: equation sets and test cases, J. Comp. Phys. 227 (8) (2008) 3849–3877.
[19] D. Gottlieb, J.S. Hesthaven, Spectral methods for hyperbolic problems, J. Comput. Appl. Math. 128 (2001) 83–131.
[20] F.F. Grinstein, L.G. Margolin, W.J. Rider, Implicit Large Eddy Simulation: Computing Turbulent Fluid Dynamics, Cambridge University Press, New York, 2007.
[21] F.F. Grinstein, C. Fureby, Recent progress on MILES for high Reynolds number flows, J. Fluids Eng. 124 (2002) 848–861.
[22] J.L. Guermond, J. Shen, Velocity-correction projection methods for incompressible flows, SIAM J. Numer. Anal. 41 (1) (2003) 112–134.
[23] A. Harten, B. Engquist, S. Osher, S.R. Chakravarthy, Uniformly high-order accurate essentially non-oscillatory schemes III, J. Comp. Phys. 71 (1987) 231.
[24] J.S. Hesthaven, A stable penalty method for the compressible Navier–Stokes equations: II. One-dimensional domain decomposition schemes, SIAM J. Sci. Comput. 18 (3) (1997) 658–685.
[25] J.S. Hesthaven, D. Gottlieb, A stable penalty method for the compressible Navier–Stokes equations: I. Open boundary conditions, SIAM J. Sci. Comput. 17 (3) (1996) 579–612.
[26] J.S. Hesthaven, R.M. Kirby, Filtering in Legendre computation, Math. Comput. 77 (263) (2008) 1425–1452.
[27] S. Hickel, N.A. Adams, J.A. Domaradzki, An adaptive local deconvolution method for implicit LES, J. Comp. Phys. 413 (2006) 436.
[28] J.O. Hinze, Turbulence, McGraw-Hill Book Company, 1975.
[29] G.-S. Karamanos, G.E. Karniadakis, A spectral vanishing viscosity method for large-eddy simulations, J. Comput. Phys. 163 (2000) 22–50.
[30] G.E. Karniadakis, M. Israeli, S.A. Orszag, High-order splitting methods for the incompressible Navier–Stokes equations, J. Comp. Phys. 97 (1991) 414–443.
[31] R.H. Kraichnan, Eddy viscosity in two and three dimensions, J. Atmos. Sci. 33 (1976) 1521.
[32] M. Lesieur, New trends in large-eddy simulations of turbulence, Annu. Rev. Fluid Mech. 28 (1996) 45–82.
[33] J.G. Levin, M. Iskandarani, D.B. Haidvogel, A spectral filtering procedure for eddy-resolving simulations with a spectral element ocean model, J. Comp. Phys. 137 (1997) 130–154.
[34] C. Meneveau, J. Katz, Scale-invariance and turbulence models for large eddy simulations, Annu. Rev. Fluid Mech. 32 (2000) 1–32.
[35] P. Meunier, P.J. Diamessis, G.R. Spedding, Self-preservation of stratified momentum wakes, Phys. Fluids 18 (2006). Article No. 106601.
[36] A.S. Monin, A.M. Yaglom, Statistical Fluid Mechanics: Mechanics of Turbulence, vol. II. The MIT Press, Cambridge, Massachusetts, 1981.
[37] U. Piomelli, Large-eddy simulations: achievements and challenges, Prog. Aero. Sci. 35 (1999) 335.
[38] S.B. Pope, Turbulent Flows, Cambridge University Press, Cambridge, 2000.
[39] P. Rosenberg, A. Fournier, P. Fischer, A. Pouquet, Geophysical-astrophysical spectral-element adaptive refinement (GASpAR): object-oriented h-adaptive fluid dynamics simulation, J. Comp. Phys. 215 (16) (2006) 59–80.
[40] K. Shahbazi, P.F. Fischer, C.R. Ethier, A high-order discontinuous Galerkin method for the unsteady incompressible Navier–Stokes equations, J. Comp. Phys. 222 (2007) 391–407.
[41] P.K. Smolarkiewicz, L.G. Margolin, MPDATA: a finite-difference solver for geophysical flows, J. Comp. Phys. 140 (1998) 459–480.
[42] G.R. Spedding, F.K. Browand, A.M. Fincham, Turbulence, similarity scaling and vortex geometry in the wake of a towed sphere in a stably stratified fluid, J. Fluid Mech. 314 (1996) 53–103.
[43] M. Stastna, K.G. Lamb, Vortex shedding and sediment resuspension associated with the interaction of an internal solitary wave and the bottom boundary layer, Geophys. Rev. Let. 14 (9) (2002) 2987–2999.
[44] P.K. Sweby, High resolution schemes using flux limiters for hyperbolic conservation laws, SIAM J. Numer. Anal. 21 (1984) 995.
[45] H. Tennekes, J.L. Lumley, A First Course in Turbulence, The MIT Press, 1972.
[46] A.A. Townsend, The Structure of Turbulent Shear Flow, second ed., Cambridge University Press, 1976.
[47] K.B. Winters, E.A. D'Asaro, Two-dimensional instability of finite amplitude internal gravity wave packets near a critical level, J. Geophys. Res. 94 (C9) (1989) 12709–12719.
[48] X. Yang, J.A. Domaradzki, Large eddy simulations of decaying rotating turbulence, Phys. Fluids 16 (2004) 4088–4104.
[49] S.T. Zalesak, Fully multidimensional flux-corrected transport algorithms for fluids, J. Comp. Phys. 31 (1979) 335.